Drude conductivity of a granular metal

Perkins, David; Smith, Robert

Journal Pre-proof

Wayside acoustic detection of train bearings based on an enhanced spline-kernelled chirplet transform

Dingcheng Zhang, Mani Entezami, Edward Stewart, Clive Roberts, Dejie Yu, Yaguo Lei

Please cite this article as: D. Zhang, M. Entezami, E. Stewart, C. Roberts, D. Yu, Y. Lei, Wayside acoustic detection of train bearings based on an enhanced spline-kernelled chirplet transform, *Journal of Sound and Vibration* (2020), doi: https://doi.org/10.1016/j.jsv.2020.115401.

This is a PDF file of an article that has undergone enhancements after acceptance, such as the addition of a cover page and metadata, and formatting for readability, but it is not yet the definitive version of record. This version will undergo additional copyediting, typesetting and review before it is published in its final form, but we are providing this version to give early visibility of the article. Please note that, during the production process, errors may be discovered which could affect the content, and all legal disclaimers that apply to the journal pertain.

Dingcheng Zhang: Writing- Original draft preparation, methodology, software, validation, formal analysis

Mani Entezami: Supervision, investigation, data curation

Edward Stewart: Supervision, Writing- Reviewing and Editing,

Clive Roberts: Supervision, resource, visualization, project administration

Dejie YU: Conceptualization

Yaguo Lei: Project administration, Writing- Reviewing and Editing,

Wayside Acoustic Detection of Train Bearings Based on An Enhanced Spline-Kernelled Chirplet Transform

Dingcheng Zhang[1]*, Mani Entezami[1], Edward Stewart[1], Clive Roberts[1], Dejie YU[2], Yaguo Lei[3]

1. School of Engineering, University of Birmingham, Birmingham, B152TT, United Kingdom
2. State Key Laboratory of Advanced Design and Manufacturing for Vehicle Body, Hunan University, Changsha, 410082, China
3. Key Laboratory of Education Ministry for Modern Design and Rotor-Bearing System, Xi'an Jiaotong University, Xi'an 710049, China

Abstract: Wayside acoustic detection is an effective and economical technology for fault diagnosis of train bearings. However, the technology has two main problems: Doppler Effect distortion, and high-level noise interference particularly harmonic interference. To solve both problems, a novel wayside acoustic detection scheme using an enhanced spline-kernelled chirplet transform (ESCT) method is proposed in this paper. Combining the spline-kernelled chirplet transform, built-in criterions, and a variable digital filter, the ESCT method is proposed for use in the extraction of the main harmonic components and corresponding instantaneous frequencies (IFs). This way, the residual signal, free of harmonic interference, can be obtained by excluding harmonic components in the raw acoustic signal using the ESCT method. The excluded harmonic components can be used to obtain motion parameters of the test train using a new estimation method. A resampling time vector can be constructed based on the estimated motion parameters. Doppler Effect in the residual signal can be reduced by using the time-domain interpolation resampling (TIR) method. Finally, spectral kurtosis (SK) is applied to extract train bearing fault features from the Doppler-free signal. By observing the Hilbert envelope spectrum of the filtered signal, train bearing faults can be detected. Comparing this approach with other schemes, the proposed solution requires comparatively little prior information and is easily applied to existing detection systems. The simulation and field experiments were conducted in this paper and results verified the effectiveness of the proposed method.

Keywords: Railway, bearing, wayside acoustic detection, Doppler Effect, enhanced spline-kernelled chirplet transform (ESCT)

*Corresponding author. Tel.: +44 07422941910;
E–mail address: railcm@contacts.bham.ac.uk (Dingcheng Zhang)

1 Introduction

Train bearings, as one of the key components of a train, need to support the whole weight of the train and also to operate at high speeds. This makes them susceptible to developing faults. In order to avoid economic loss associated with increased maintenance requirements and non-availability of trains, condition monitoring for train bearings is beneficial. Wayside acoustic detection is an effective and economical technology for train bearing analysis as a single monitoring station can be used to evaluate multiple trains with no requirement for access to the track or rolling stock to install the equipment. However, there are two main problems with wayside acoustic detection: signal distortion associated with the Doppler effect, and the presence of high levels of noise, particularly harmonic interference [1-3]. Acoustic signals collected from test trains are distorted by Doppler Effect because of the relative motion between trains and microphones. The Doppler Effect results in serious frequency-domain distortion to the collected signals. In addition, collected signals often include high levels of background noise such as vehicle noise, environmental noise, or aerodynamic noise, etc. Furthermore, they are also susceptible to harmonic interference generated by other moving or rotating machine components in the train.

To reduce the Doppler Effect on the wayside acoustic signal, researchers have proposed many methods [4-7]. The time-domain interpolation resampling (TIR) method is one kind of most used methods to reduce Doppler Effect. According to different ways for obtaining the resampling vector, the TIR method can be divided into two main categories: instantaneous frequency (IF) based and motion parameter based methods. The core of the IF-based method is to extract IFs of acoustic signals generated by the target bearing. The extracted IF can be used to calculate the resampling time vector. Some research works about the IF-based method have been published [4, 8] and good results were demonstrated. However, the collected wayside acoustic signals include high level background noise. It is hard to extract IF of the sound signal generated by the target bearing. Furthermore, the IFs of characteristic fault frequencies are difficult to identify, which limits its application [7]. Central to the motion parameter based method is the estimation of motion through the use of a Doppler distorted correlation model. Doppler Effect reduction methods based on motion parameters have been successfully applied in wayside acoustic detection [9-11]. However, this kind of methods is difficult to meet requirements of real application because the model construction is a time-consuming process [12].

Recently, time-frequency (TF) methods such as short-time Fourier transform (STFT) [13,

14], pseudo time-frequency analysis (PTFA) [15], and time-frequency data fusion (TFDF) [16] etc., have been applied to extract IFs from wayside acoustic signals. These methods perform well in some cases, but are generally restricted by the Heisenberg uncertainty principle or unexpected cross-term [17, 18], they suffer from TF resolution issues, and hence can have poor IF extraction performance for non-linear and non-stationary signals. Some advanced post-processing methods have been proposed to improve TF resolution; these can be classified into two kinds: non-parameterised and parameterised TF methods. The non-parameterised TF methods, such as the reassignment method [19], synchrosqueezing transform [20] and synchroextracting transform [21], have the ability to process the TF coefficients using conventional time-frequency analysis, however these methods are sensitive to noise. Therefore, the non-parameterized TF methods are not appropriate for use in wayside acoustic detection systems for train bearing faults. The parameterised TF methods, such as the polynomial chirplet transform [22], generalised warblet transform [23] and spline-kernelled chirplet transform (SCT) [24], are designed to improve the energy concentration of the TF result by demodulating the time-varying signal. The parameterised TF methods can adapt to different kinds of TF patterns, linear / nonlinear or periodic / non-periodic, by using an appropriate generalised kernel function. The SCT method is suited to the analysis of mono-component signals with complex IFs as it uses low-degree piecewise polynomials. Due to the Doppler Effect, the IF of the acoustic signal for the target bearing has significant distortion at the point where the sound source passes the microphone. The SCT method can be adapted to identify these distorted IF in the acoustic signals. However, wayside acoustic signals associated with train bearings normally have multiple harmonic components which interfere with each other. Further to this, both the start and end of an IF are likely to be significantly affected by noise. The SCT method, therefore, is limited in that it is unable to extract the IFs associated with the multiple harmonic components found in train bearing signals; and while the region of the IF useful for motion parameter estimation is not as impacted by noise as the start and end sections, it's successful identification is dependent on these regions which are more affected.

To overcome the problems described above, a new scheme for wayside acoustic detection based on harmonic component extraction is proposed in this paper. The scheme combines SCT, built-in criterion and a variable digital filter (VDF), to produce an enhanced spline-kernelled chirplet transform (ESCT) method. This method is suitable for extracting IFs of harmonic components while also obtaining a residual signal that does not include them. The motion parameters of the train being inspected can be obtained by using an estimation

method proposed in [25]. The residual signal is then resampled using a resampling time vector derived from these motion parameters to reduce the Doppler Effect. Finally, the spectral kurtosis (SK) was applied to the residual signal and the filtered signal including fault information can be obtained. Through observing the Hilbert envelope spectrum of the filtered signal, bearing faults can be detected. To demonstrate the advantage of the proposed method, the multi-scale chirplet path pursuit (MSCPP) method which is widely applied to the extraction of IF curves [26, 27] is compared with the ESCT method.

This paper is organised as follows: A novel scheme proposed in this work is introduced in section 2. The simulation and field experiments are conducted and results are shown in section 3 and 4. The final section the conclusions of the paper.

2 A wayside acoustic detection scheme based on an enhanced spline-kernelled chirplet transform

Wayside acoustic recordings of train axle bearings contain strong harmonic interference and background noise which can contribute to both misdiagnosis and missed-diagnosis. Additionally, Doppler Effect distortion is an intractable problem in extracting fault feature information from the collected signals. To address these issues, a novel scheme based on an enhanced spline-kernelled chirplet transform method is proposed and introduced for use with wayside acoustic fault detection for train bearings. The proposed method consists of three main procedures whish are described in the remainder of this paper: 1) extracting IFs and filtering corresponding harmonic components; 2) estimating motion parameters based on the obtained IFs and reducing the Doppler Effect in the residual signal; 3) extracting fault feature signals commonly associated with impulsive components, and detecting faults. A flow chart illustrating the proposed scheme is shown in Fig. 1.
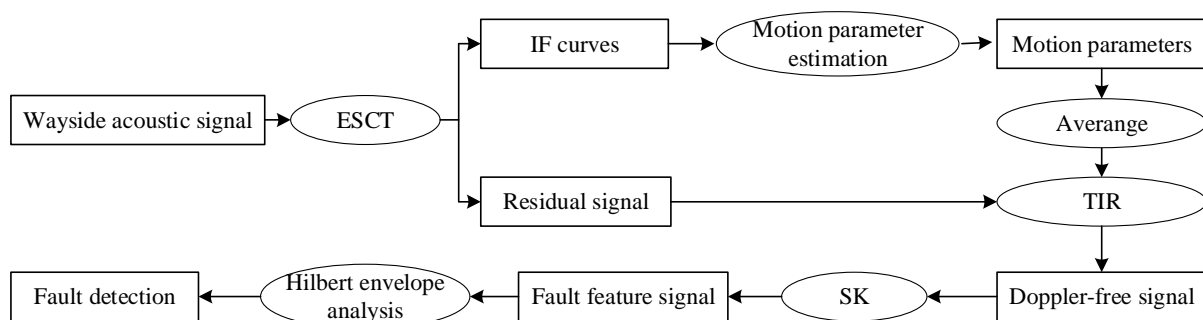

Fig. 1 Flow chart of the proposed scheme

2.1 Motion parameter estimation

A schematic diagram of Doppler Effect generation of the sound source in railway vehicles is described in Fig. 2 . v is the speed of the train (the speed is considered as a constant because the time for a train passing the microphone is short); c is the speed of sound; s is the longitudinal distance between the sound source and the microphone. r is the perpendicular distance between the sound source and the microphone. d is the distance between the sound source and the microphone. Values of s, r and d are changed with time. t_c is the time point when s is equal to 0, that is, when the sound source is at the closest point of approach (CPA). If a sound source generates the acoustic signal at time τ, the microphone will collect the signal section at time t.

To reduce Doppler Effect in wayside acoustic signal, the core of the TIR method [28] is constructing the resampling time vector, $\mathbf{t_r}$, as demonstrated in Eq. (1).

$$\mathbf{t_r} = \mathbf{t} + \frac{\sqrt{r^2 + (s - v\mathbf{t})^2}}{c} \tag{1}$$

According to Eq. (1), the resampling time vector, $\mathbf{t_r}$, can be estimated if the motion parameters (r, s, v, c) are identified. Fig. 3 is the basic layout of the wayside acoustic detection system used in this work. There are a sonic anemometer, a pair of light-gates, data recording equipment and only one microphone. The light-gates are used to identify the target bearing and record the CPA time of the target bearing, t_{ct}. c and r can be measured directly. Hence, $\mathbf{t_r}$ can be constructed after estimating motion parameters (v, s).

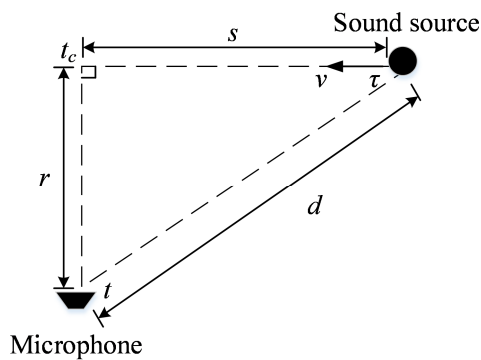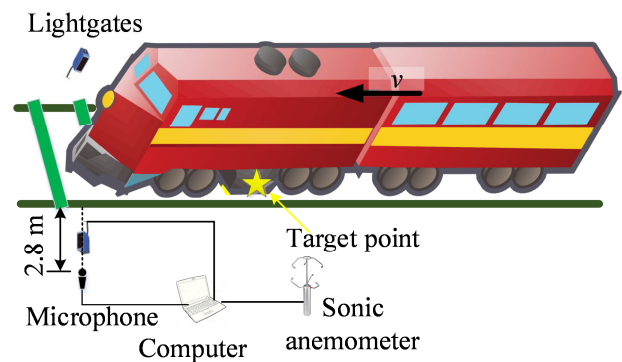Fig. 2 Schematic diagram of a wayside acoustic detection system

Fig. 3 Basic layout of the wayside acoustic detection system used in this work

Many researchers focus on the motion parameter estimation for moving objects. An estimation method, proposed by Timlelt et al., makes use of extracted IF curves [25]. This method is a closed-form solution which is less complex than conventional methods, and thus

more suitable for hardware implementation. The derivative of an IF curve from an acoustic signal such as those recorded in this work, and including the Doppler Effect, is given in Eq. (2).

$$\dot{f}(t)=\frac{v^2r^2(c^2\text{-}v^2)f(t_c)}{\sqrt{[r^2(c^2\text{-}v^2)+v^2c^2(t^2\text{-}t_c{}^2)]^3}} \tag{2}$$

Eq. (2) shows that $\dot{f}(t)$ is less than zero, and hence the IF curve when distorted by the Doppler Effect has a monotonically decreasing trend. Eq. (3) states that $\hat{t}_c$ is the estimated value of the time when a sound source (which may not necessarily be the target bearing) passes the microphone. An estimate for the speed of that sound source, $\hat{v}$, is given in Eq. (4)

$$\hat{t}_c=\text{Arg max}\left|\dot{f}(t)\right| \tag{3}$$

$$\hat{v}=\sqrt{\frac{\sum_{t=1;t\neq\hat{t}_c}^{N}c^2\left[(t\text{-}\hat{t}_c)\dot{f}(\hat{t}_c)\right]^2[f(\hat{t}_c)\text{-}f(t)]^2}{\sum_{t=1;t\neq\hat{t}_c}^{N}\left(\left[(t\text{-}\hat{t}_c)\dot{f}(\hat{t}_c)\right]^2\text{-}[f(\hat{t}_c)\text{-}f(t)]^2\right)\dot{f}(\hat{t}_c)^2}} \tag{4}$$

It is usual for multiple harmonic components to exist in an acoustic signal recorded during the passage of a train. These are generated by different sound sources which would include, but not be limited to, the target bearing. The different harmonic components, $f_{i=1,2,\cdots,n}(t)$, each have their own IF curves. Considering these components as per Eq. (3) and Eq. (4), leads to a range of slightly different estimations of train speed, $\hat{v}_{i=1,2,\cdots,n}$. An average is then used to reduce the non-systematic error in the estimated speed values. Hence, an accurate estimate of train speed, $\hat{v}_a$, can be obtained. Accordingly, the initial distance between the start point of the detection region and the microphone, $\hat{s}$, is estimated as shown in Eq. (5).

$$\hat{s}=\hat{v}_a(t_{ct}\text{-}t_0) \tag{5}$$

where t_{ct} is identified by the light-gates and t_0 is the initial time when the target bearing enters the detection zone. The details for determining t_0 are introduced in Section 4. Hence, $\mathbf{t_r}$ can be obtained by substituting the estimated motion parameters $(\hat{v}_a,\hat{s})$ into Eq. (1). Doppler Effect in wayside acoustic signals can be reduced by using the TIR method.

2.2 Multiple harmonic component extraction based on ESCT

2.2.1 Spline-kernelled chirplet transform

According to [24], the Spline-kernelled Chirplet Transform (SCT) performs well when extracting nonlinearly time-varying IF curves from signals. The SCT method essentially

includes three procedures: 1) frequency-rotated operating; 2) frequency-shifted operating and 3) the short time Fourier transform. The SCT of a signal $x(t) \in L^2(R)$ is defined as per Eq. (6).

$$\text{SCT}(\tau,\omega,\mathbf{Q},\sigma)= \int_{-\infty}^{+\infty} \bar{z}(t)\omega_\sigma(t\text{-}\tau)\exp(\text{-j}\omega t)\,\text{dt} \qquad \text{s.t.} \quad \tau \in (t_i,t_{i+1}) \tag{6}$$

where τ stands a certain time. Suppose the time duration of the analysis signal, t, is belong to an interval $[a,b]$, i.e. $a=t_1 < \cdots < t_{l+1}=b$. t_i is the broken point of time, $i=1, \cdots, l$. $\omega_\sigma(t)$ is the Gaussian window function, as shown in Eq. (7); $z(t)$ is the analytical signal of $x(t)$ subjected to the Hilbert transform H, i.e. $z(t)=x(t)+H[x(t)]$, hence $\bar{z}(t)$ is constructed as shown in Eq. (8). In Eq. (8), $\phi^R(t,\mathbf{Q})$ and $\phi^s(t,\tau,\mathbf{Q})$ are frequency-rotated and frequency-shifted operators, which are given by Eq. (9) and Eq. (10), respectively.

$$\omega_\sigma = \frac{1}{\sqrt{2\pi\sigma}} \exp\left(-\frac{1}{2}\left(\frac{t}{\sigma}\right)^2\right) \tag{7}$$

$$\bar{z}(t)=z(t)\phi^R(t,\mathbf{Q})\phi^s(t,\tau,\mathbf{Q}) \tag{8}$$

$$\phi^R(t,\mathbf{Q})=\exp\left(-j\sum_{k=1}^{n}\frac{q_k^i}{k}(t\text{-}t_i)^k+\gamma_i\right) \tag{9}$$

$$\phi^s(t,\tau,\mathbf{Q})=\exp\left(j\sum_{k=1}^{n}q_k^i(\tau\text{-}t_i)^{k\text{-}1}t\right) \tag{10}$$

where n is the order of spline. The frequency-rotated operation is used to rotate the analysis signal by adding the IF of $\phi^R(t,\mathbf{Q})$, i.e. $\Omega_R(t)=-\sum_{k=1}^{n} q_k^i(t\text{-}t_i)^{k\text{-}1}$, in the time-frequency domain. The frequency-shifted operator is used to further shift the signal by adding the frequency of $\phi^s(t,\tau,\mathbf{Q})$ at τ, i.e. $\Omega_S(\tau)=\sum_{k=1}^{n} q_k^i(\tau\text{-}t_i)^{k\text{-}1}$.

Actually, the spline kernel in the frequency-rotate and frequency-shift operators is constructed from a set of piecewise polynomial functions with boundary constraints defined at jointed breaks. A spline of order n can be defined in piecewise polynomial form [29] (with l pieces), as shown in Eq. (11). In Eq. (9) and Eq. (10), $\mathbf{Q}(i,k)=q_k^i$ refers to the local polynomial coefficient matrix of the spline kernel, and γ_i satisfies Eq. (12) for the initial case where $\gamma_1 = 0$.

$$S(t)=\sum_{k=1}^{n} q_k^i(t\text{-}t_i)^{k\text{-}1} \qquad \text{s.t.} \quad t\in(t_i, t_{i+1}) \quad i\in[1,l] \tag{11}$$

$$\gamma_i\text{-}\gamma_{i+1}=\sum_{k=1}^{n}\frac{q_k^{i+1}}{k}(t_i\text{-}t_{i+1})^k \tag{12}$$

By using an iterative optimization of the spline function [24], a complex IF curve can be estimated using the SCT method by searching for energy ridges on a time-frequency map. Comparing this with other kinds of general parameterized time-frequency transform (GPTF) method, SCT is more suited to the estimation of the IF curve of the Doppler-shift signal due to its rapidly varying nature. To demonstrate this, a mono-component signal with Doppler Effect is simulated as per the acoustic theory described in [30]. The parameters for the simulated signal are demonstrated in Tab. 1. The resulting extracted IF curves, using STFT, SCT, a polynomial chirplet transform, and a generalised warblet transform are shown in Fig. 4 (a), (b), (c) and (d), respectively. The figure indicates that the GPTF methods (the latter 3) all concentrate the energy on the frequency axis of the time-frequency domain plot, but the SCT method has a more substantial effect during the more rapidly changing region of the IF. Fig. 4 (e) shows the original IF curve used to generate the simulated signal and the estimated IF curves based on the three GPTF methods. Although all of IF curves estimated by the GPTF methods have minor differences from the original, the IF curve estimated by the SCT method minimises this variation. This is significant in the further estimation of the motion parameters.

Tab. 1 Parameters for the simulated signal

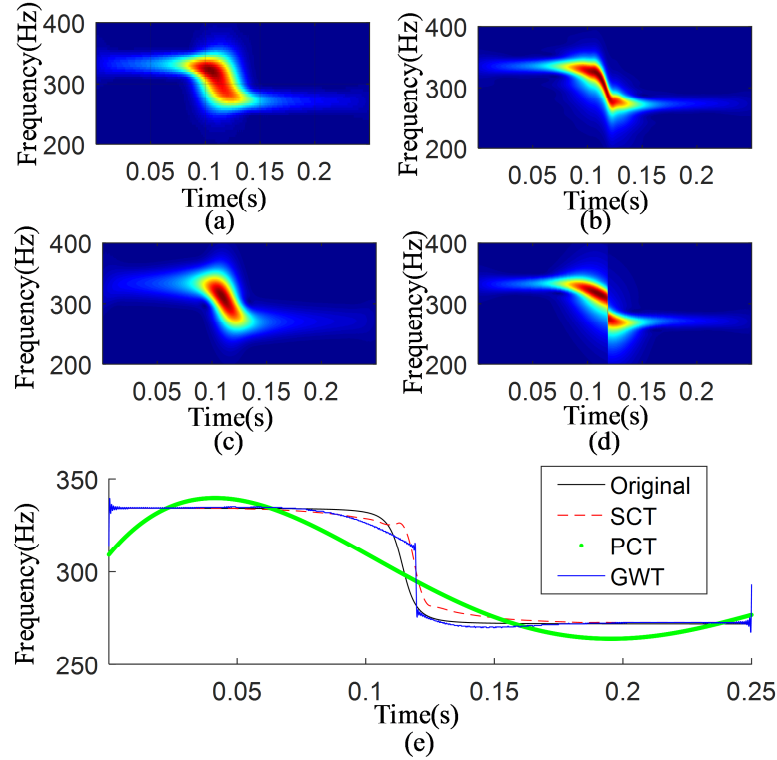| s	r	c	v	A	f_0
4 m	0.2 m	340 m/s	35 m/s	1	300 Hz

Fig. 4. (a) STFT result, (b) SCT result, (c) Polynomial Chirplet Transform result, (d) Generalised Warblet Transform result, (e) IF curves

2.2.2 Built-in criterions of the ESCT method

Although the SCT method is a powerful tool for estimating IF curves, it is limited in a number of ways which affect its suitability for practical, real-world, use [31]. Literature [31] introduces an improved method to overcome one of these limitations through dividing the original signal into a number of time segments of equal interval. This method has been shown to be successfully applied to fault diagnosis in wind turbines. Unfortunately, however, the method is unable to extract harmonic components that have been distorted by the Doppler Effect in wayside acoustic recordings of train bearings for a number of reasons:

- The key section of the harmonic component of the wayside acoustic signal is short. As described in [31], the SCT method cannot identify the births and the deaths of short harmonic components;

- Methods based on time-domain fitting are unsuitable for analysing wayside acoustic signals with high levels of noise or significant interference from other components.

To solve these problems, a novel Enhanced Spline-kernelled Chirplet Transform (ESCT) is proposed in this paper. The energy contribution coefficient θ_i is proposed to identify birth

and death points of the IF curves in the time-frequency map in Eq. (18). The value of θ_i is directly decided by the energy of the i-th point in the IF component. The lesser the energy at i-th point is, the greater θ_i is. For one IF, the vector of the energy contribution coefficient is expressed as $\boldsymbol{\theta}=(\theta_1,\theta_2,\cdots\theta_N)$. $\hat{\boldsymbol{\theta}}$ in Eq. (19) is the normalised vector of $\boldsymbol{\theta}$.

$$\theta_i = \frac{\mathrm{E}\left(\mathrm{TFR}\left(\mathbf{IF}_{j=1,2,\cdots N,\ j \neq i}\right)\right)}{\mathrm{E}\left(\mathrm{TFR}\left(\mathbf{IF}_{1,2,\cdots,N}\right)\right)} \tag{13}$$

$$\hat{\boldsymbol{\theta}} = \frac{\boldsymbol{\theta} - \boldsymbol{\theta}_{\min}}{\boldsymbol{\theta}_{\max} - \boldsymbol{\theta}_{\min}} \tag{14}$$

where $\mathbf{IF}_{j=1,2,\cdots,N}$ is the IF vector, TFR($\bullet$) is the amplitude of result using the SCT method, E($\bullet$) is the energy of a vector, $\boldsymbol{\theta}_{\max}$ and $\boldsymbol{\theta}_{\min}$ are the maximum and minimum values in $\boldsymbol{\theta}$ respectively.

Hence, based on the behaviour of the signal as influenced by the Doppler Effect, the built-in criterions shown in Eq. (15) and Eq. (16) are proposed to identify the birth and death of the IF curve in the time-frequency domain.

Criterion 1:

$$\mathrm{TRF}(\mathbf{IF}_{i,j}) \geq \boldsymbol{\theta}\mathrm{M}(|\mathrm{TRF}(\mathbf{IF}_i)|) \tag{15}$$

Criterion 2:

$$\mathbf{IF}'_{i,j} < 0 \tag{16}$$

where i is the number of IF curve and j is the number of point at the i-th IF curve, $\mathbf{IF}'_{i,j}$ is the first-order derivative of the IF curve $\mathbf{IF}_{i,j}$, $|\blacksquare|$ and M($\blacksquare$) are the absolute and mean operations, respectively.

For each IF curve, the TFR sections with minor values are easily distorted by noise and other IF components. Hence, the first criterion is used to exclude the sections of IF curves with minor amplitude values in the TFR. The second criterion is constructed according to Eq. (2) because the IF curves caused by the Doppler Effect are monotonically decreasing.

To demonstrate the effectiveness of the built-in criterions, a simulated signal with an SNR (signal-to-noise ratio) of -10 dB is constructed according to the basic theory of Doppler Effect described in [30]. Parameters of the simulated signal are shown in Tab. 1. The TFR of the simulated signal obtained by using SCT with initialized parameters is shown in Fig. 5 (a), where the black line represents the energy ridge. Fig. 5 (a) shows that the sections of the IF with smaller amplitude (lower energy) are more significantly affected by noise. In Fig. 5 (b),

the black solid line is the amplitude of the energy ridge in the TFR and the red dashed line is the threshold based on the energy contribution coefficient as described in Eq. 15. Fig. 5 (b) shows that smaller thresholds correspond to larger energy ridge amplitudes. Combining both built-in criterions, the significant portion of the IF can be identified, which is indicated by the dark line in the Fig. 5 (c). It can be seen from the figure that the significant portion of the IF is monotonically decreasing. Fig. 5 (d) is then the result of the SCT method applied to the significant portion of the IF component. The figure indicates the importance of the built-in criterion and the benefit of first extracting the significant portion of the IF curve, particularly from signals with high levels of noise. It should be noted that the unit of amplitude of the acoustic signal, shown in Fig.5 (b) and in other figures throughout the paper, is kpa.
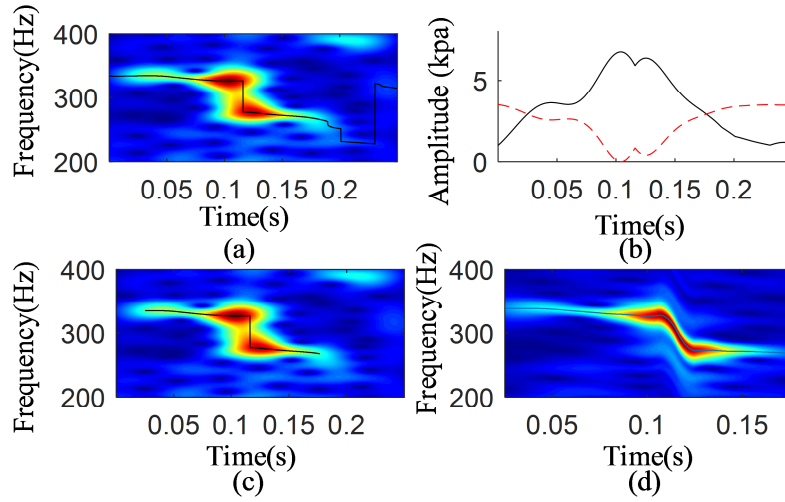

Fig. 5 (a) SCT-based TFR with initialized parameters and the energy ridge shown (black line), (b) The IF's amplitude (black) and corresponding threshold (red dash), (c) SCT-based TFR with initialized parameters and the energy ridge shown (black line) for the significant IF portion only, (d) the result of the ESCT method

2.2.3 Multiple harmonic component extraction using the ESCT method

A strategy introduced in [32] is used in this paper to extract IF curves of multiple harmonic components from raw signals. The method essentially involves extracting IF curves one-by-one with the curves with the highest TRF energy extracted first. Then, a variable digital filter (VDF) is then constructed to exclude the corresponding harmonic components one-by-one from the raw signal [33]. The significant portions of the IFs are used to identify the centre frequencies for the VDFs. The basic procedure of VDF is described in Eq. (17)-(20).

$$Y_1(\omega) = X(\omega) H_{t'}(\omega) \tag{17}$$

$$Y_2(\omega) = \exp(-i\omega(N+1)) Y_1(\omega) \tag{18}$$

$$Y_3(\omega) = Y_2(\omega)H_{t'}(\omega) \tag{19}$$

$$Y(\omega) = \exp\left(-i\omega(N+1)\right)Y_3(\omega) \tag{20}$$

where $X(\omega)$ is the frequency response of the original signal, $H_{t'}(\omega)$ is the VDF at a certain time, and $Y(\omega)$ is the frequency response of the filtered signal. A Chebyshev □ filter is selected as the base filter used in this paper because its amplitude response function is steep in the transition band and decreases monotonously. The bandwidth of the VDF is selected to be 15 Hz based on an analysis of a range of possible filter configurations.

Unlike the conventional SCT method, the ESCT method can be used to extract multiple IFs and corresponding signal components. In addition, the ESCT can identify births and deaths of IFs in order to avoid interference arising from noise. The flow chart shown in Fig. 6 describes the ESCT method. In the method the IF curve is first extracted using the SCT method. Two built-in criterions are then applied to obtain the significant portion of the IF curve. Next, a VDF with a centre frequency based on the significant portion of the IF is used to exclude the corresponding harmonic component. Due to significant crossover and interference between different harmonic components, the truncated IF section identified by the first criterion may not satisfy the second criterion and as such would be regarded as an interference component. This interference component is also excluded using a VDF the centre frequency of which is based on the truncated IF section identified by the first criterion. This process is repeated until the threshold is satisfied, i.e. the length of the extracted IF in the time axis is less than 1/4 of the detection period. The residual signals generated, and the significant portions of the IF curves identified, are both considered to be outputs of the ESCT method, as shown in Fig. 1.
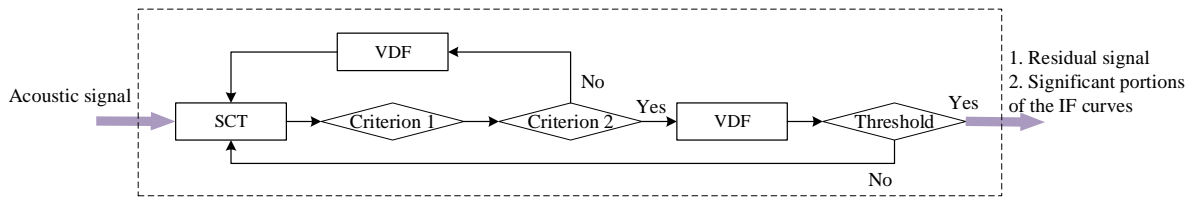

Fig. 6 Flow chart of the ESCT method

In order to demonstrate the extraction of multiple harmonic components using the ESCT method, a simulated signal including 3 harmonic components, each featuring the Doppler Effect, (i.e. x_1, x_2 and x_3) and a random noise component is constructed according to the basic theory of Doppler Effect [30]. The parameters of the harmonic components are shown in Tab. 2. Fig. 7 (a) and (b) are the time domain waveform and TFR of the simulated signal respectively. The first part of the ESCT method is applied to extract the IF curves shown as solid black lines in Fig. 7 (c). The ESCT filter component then eliminates the harmonic

components corresponding to these IF curves. Fig. 7 (d) shows representations of the harmonic components (which include the Doppler Effect) eliminated by the ESCT method's filter elements. For comparison, the same simulated signal is analysed using the Synchrosqueezing transform, Reassignment, and synchroextracting transform methods. The results shown in Fig. 8 are equivalent to the point in the ESCT process represented by Fig. 7 (c). In Fig. 8 the time-frequency energy concentration is improved, and however the energy ridges have significant distortion which makes further processing non-viable.

Tab. 2 Parameters of the harmonic components

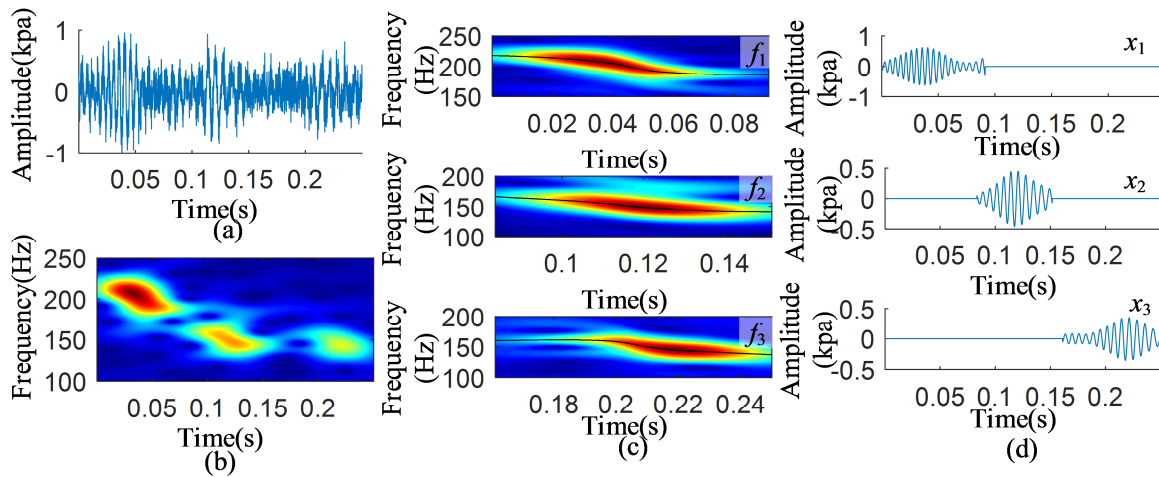|	s	r	c	v	A	f_0
x_1	1 m	0.2 m	340 m/s	25 m/s	2	200 Hz
x_2	3 m	0.2 m	340 m/s	25 m/s	1.5	150 Hz
x_3	5.5 m	0.2 m	340 m/s	25 m/s	1	145 Hz

Fig. 7. (a) Time domain waveform of the simulated signal, (b) TFR of the simulated signal, (c) IF curves obtained using the ESCT method, (d) Representation of components eliminated by the ESCT method
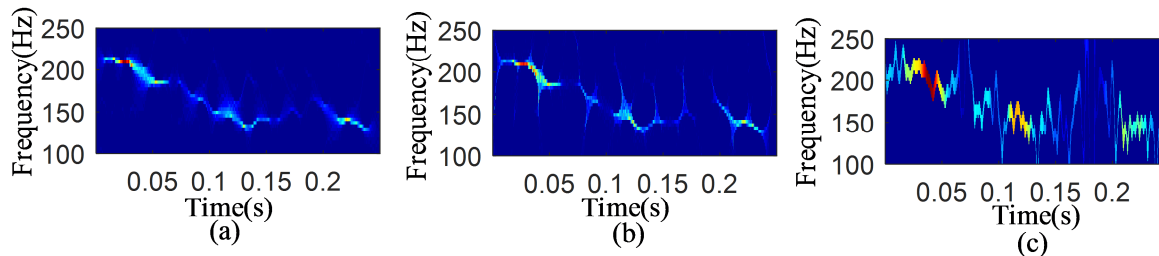

Fig. 8. Alternative processing applied to simulated signal: (a) Synchrosqueezing transform; (b) Reassignment method; (c) Synchroextracting transform.

3 Simulation experiments

A simulation test signal as described as in [13] is constructed to verify the effectiveness of the proposed method in the section. The simulated signal, x(*t*), includes 5 harmonic components ($h_{i=1\ldots5}$) with Doppler Effect, a signal with fault information s(*t*), and a random noise element n(*t*) in Eq. (21). The SNR of s(*t*) is -5 dB, the bearing fault feature frequency, f_c, is set to 120 Hz, and the motion parameters of the components in the simulated signal are given in Tab. 3. The sampling frequency is 8192 Hz and the sampling time is 0.25 s. The train speed, v, and speed of sound, c, are considered to be 35 m/s and 340 m/s, respectively.

$$x(t)=s(t)+\sum_{i=1}^{5}h_i(t)+n(t) \tag{21}$$

Tab. 3 Motion parameters of components in the simulation test signal

	h_1	h_2	h_3	h_4	h_5	s
s	2	2	4	4	4	4
r	0.5	0.8	0.5	0.5	1.2	0.5
A	1.5	1	1.5	1.8	1	0.5
tc	0.057	0.057	0.114	0.114	0.114	0.114
f_o	250 Hz	150 Hz	100 Hz	45 Hz	75 Hz	1500 Hz

The time-domain waveform, Hilbert envelope spectrum and time-frequency representations of the simulation signal are shown in Fig. 9 (a), (b) and (c), respectively. It can be seen from Fig. 9 (b) that no obvious peaks exist at f_c or its harmonics because the fault feature is masked by noise. Additionally, a significant peak exists at 3 Hz in Fig. 9 (b) due to signal amplitude attenuation [6]. Fig. 9 (c) shows that there are strong harmonic interferences in the simulation test signal. The upper part of Fig. 9 (c) shows a zoomed in view of the low-frequency region indicated by the yellow dashed box in the lower part of the figure. The ESCT method is applied to the simulated signal to extract the 5 IF curves of the harmonic components as shown in Fig. 10. In the figure, the dark lines are the extracted parts of IF curves and the red dashed lines are the corresponding parts of the simulated IF curves. The figure shows a good correlation between these elements despite the presence of the Doppler Effect in the signal components.
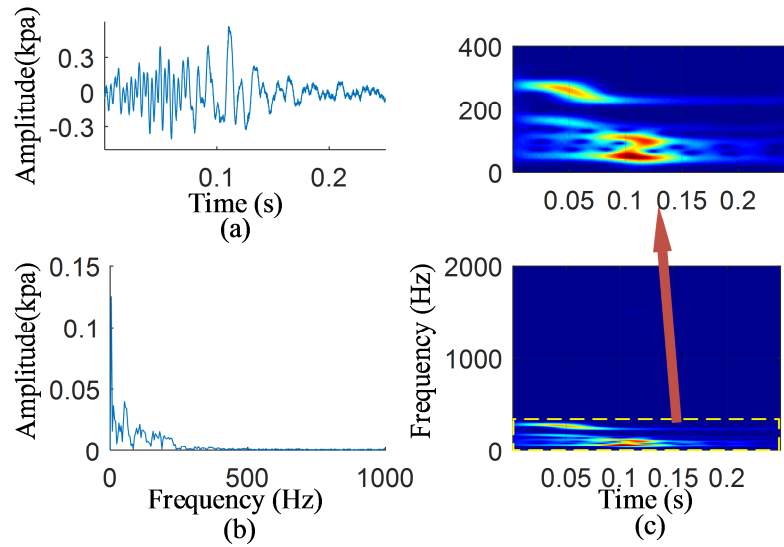
Fig. 9 simulation test signal (a) time-domain waveform, (b) the Hilbert envelope spectrum, (c) TFR
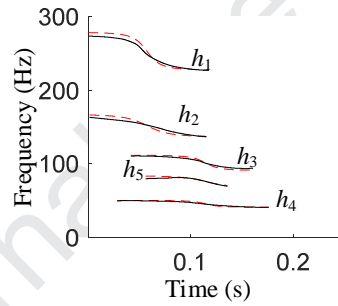

Fig. 10 IFs of the harmonic components of the simulated signal

To test the de-noise ability of the proposed method, simulated signals with different SNR values are constructed. The estimated motion parameters are shown in Tab. 4. In the table, σ is the variance of the estimated speed values for the different harmonic components, $\hat{v}(h_i)$. ε is the error ratio between the accurate estimate of train speed, $\hat{v}_a$, and the true value of the train speed, v, ($\varepsilon = |v - \hat{v}_a| / v$). σ and ε indicate the stability and accuracy of the result obtained using the ESCT method. Tab. 4 shows that either one or both of the values of σ or ε increase with increasing SNR.

Tab. 4 Estimated motion parameters obtained for simulation test signals with different SNR values

	$\hat{v}(h_1)$ m/s	$\hat{v}(h_2)$ m/s	$\hat{v}(h_3)$ m/s	$\hat{v}(h_4)$ m/s	$\hat{v}(h_5)$ m/s	σ	$\hat{v}_a$ m/s	ε %
SNR = -5	34.57	33.67	32.24	37.18	36.10	3.8	34.75	0.7
SNR = -6	34.48	38.45	33.83	36.99	39.54	6.1	36.66	4.7

SNR = -7	34.26	29.37	32.35	34.92	35.14	5.8	33.2	5.2
SNR = -8	33.76	30.96	32.42	37.45	36.67	7.6	34.25	2.1
SNR = -9	34.38	32.75	33.45	31.64	33.63	1.1	33.17	5.2
SNR = -10	34.08	28.72	33.20	35.94	35.75	8.9	33.34	4.7

Using the ESCT method, residual signals (with harmonic interferences removed) are obtained for each of the simulation test signals with different SNR values. Hence, se can be calculated according to Eq. (5). Substituting motion parameters $(\hat{v}_a, \hat{s})$ into Eq. (1), the resampling time vectors are obtained and applied using the TIR method to reduce the Doppler Effect in the residual signals. The filtered signals are then obtained from the resulting Doppler Effect-free signals using the SK method. The Hilbert envelope spectra of the filtered signals are shown in Fig. 11. The sub-figures show that there are obvious peaks at f_c or its harmonics which indicate the existence of a bearing fault. Hence, the effectiveness for the proposed method is demonstrated for differing noise levels.
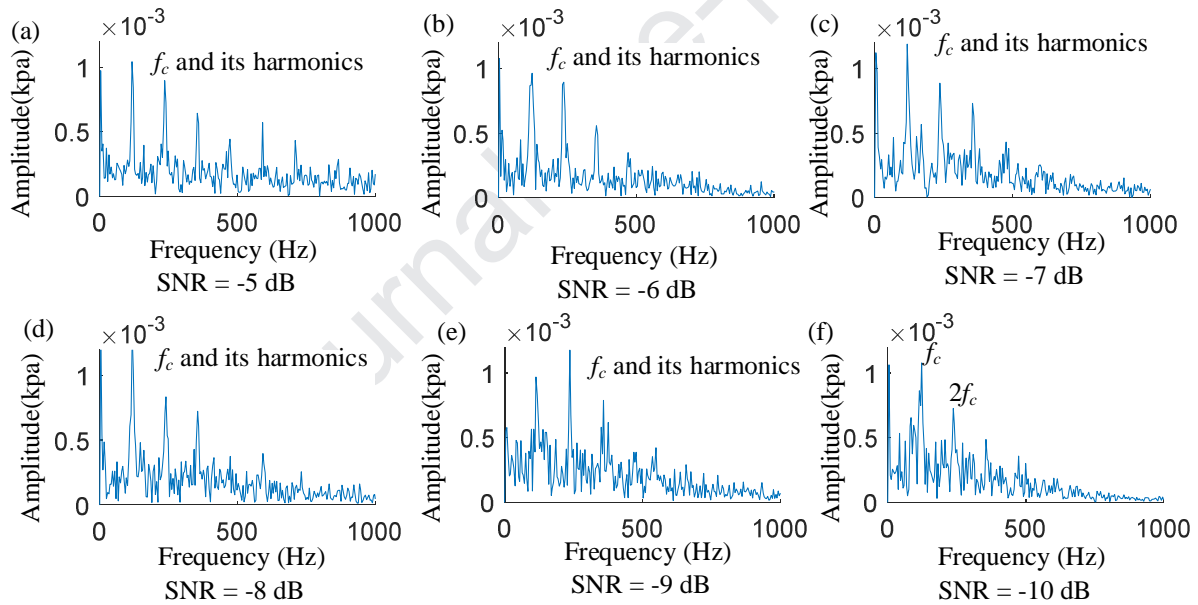

Fig. 11 Hilbert envelope spectra of the filtered signals obtained from simulation test signals with different SNR values

4 Field experiments

In the following section, two field experiments are used to demonstrate the effectiveness of the proposed scheme in a real railway environment. For safety reasons, rather than running a faulty train, a loudspeaker was fitted to the third axle of a test train and used to broadcast acoustic signals recorded in the laboratory. This, therefore, simulated a vehicle with a bearing fault passing the recording equipment, as shown in Fig. 12 (a) [34]. The rotational speed was

270 RPM approximately when recording acoustic signals in the laboratory. To align the recordings with the speed of the test rig in the lab, the test train's speed was set to 13.1 m/s approximately. The experiments were repeated with two sets of recordings, thus demonstrating the detection of both outer race and roller faults. The faulty bearings from which the recordings were taken are shown in Fig. 12 (b) and (c), respectively. The parameters of the test bearing are shown in Tab. 5. According to Eq. (22) and Eq. (23), the roller passing frequency outer race f_{RPFO} and the roller fault frequency f_{RFF} are approximately 43Hz and 35Hz. The sampling frequency used was 8192 Hz and hence the sampling time was 0.25 s.

$$f_{\mathrm{RPFO}} = \frac{n}{2}\left(1 - \frac{\mathrm{RD}}{\mathrm{PD}}\cos\beta\right)f_r \tag{22}$$

$$f_{\mathrm{RFF}} = \frac{\mathrm{PD}}{\mathrm{RD}}\left(1 - \left(\frac{\mathrm{RD}}{\mathrm{PD}}\cos\beta\right)^2\right)f_r \tag{23}$$

Tab. 5 Test bearing parameters

Type	Number of rollers n	Roller diameter RD	Pitch diameter PD	Contact angle β
TAROL 130/230-U-TVP	22	24 mm	187 mm	6.9$^{\mathrm{o}}$

In case 1, the speaker installed on the 3$^{\mathrm{rd}}$ bearing broadcasted the sound with outer race fault information. Fig. 13 (a) is the collected acoustic signal recorded during the test. In the figure, the black line corresponds to the signal collected from the light-gate. A section of the collected signal is selected as the "analysis signal" for the 3$^{\mathrm{rd}}$ bearing as shown in Fig. 13 (b). The analysis signal corresponds to the time when the 3$^{\mathrm{rd}}$ bearing passes the microphone, t_c=5.617s. The detection period includes 2048 sample points, which are divided into two parts, L1 and L2, based on the triggering of the light-gate signal. L1 is the 800 sample section before the bearing passing the light gate, while the remaining 1248 samples that occur after the light gate are known as L2. The time intervals of L1 and L2, t_{L1} and t_{L2}, are hence 0.098 s and 0.152 s, respectively. t_0 (as used in Eq. (5)) is equal to 5.519 s, i.e. $t_0 = t_c - t_{\mathrm{L1}}$. The Hilbert envelope spectrum of the signal being analysed is shown in Fig. 13 (c). There are no obvious peaks at f_{RPFO} or its harmonics, which results in miss-diagnosis. Fig. 13 (d) is the TFR of the analysis signal. The figure shows that multiple harmonic components exist in the low frequency zone of the TFR of the analysis signal.

(a)

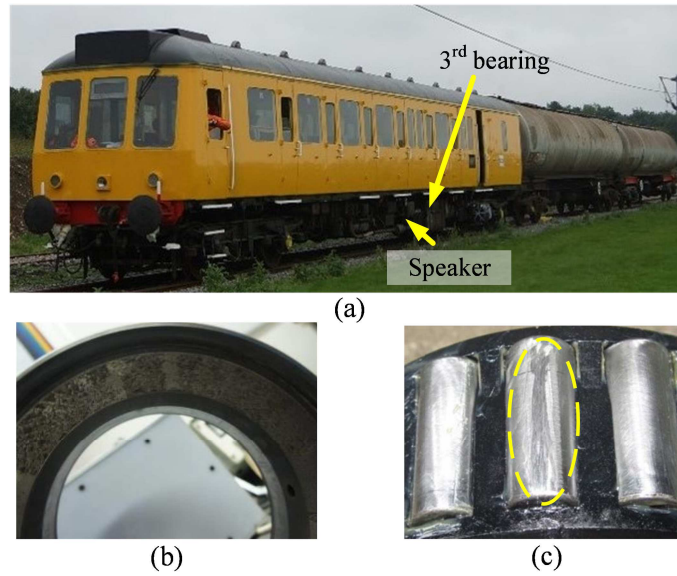(b)   (c)

Fig. 12 (a) Test train, (b) Test bearing with outer race fault, (c) Test bearing with roller fault
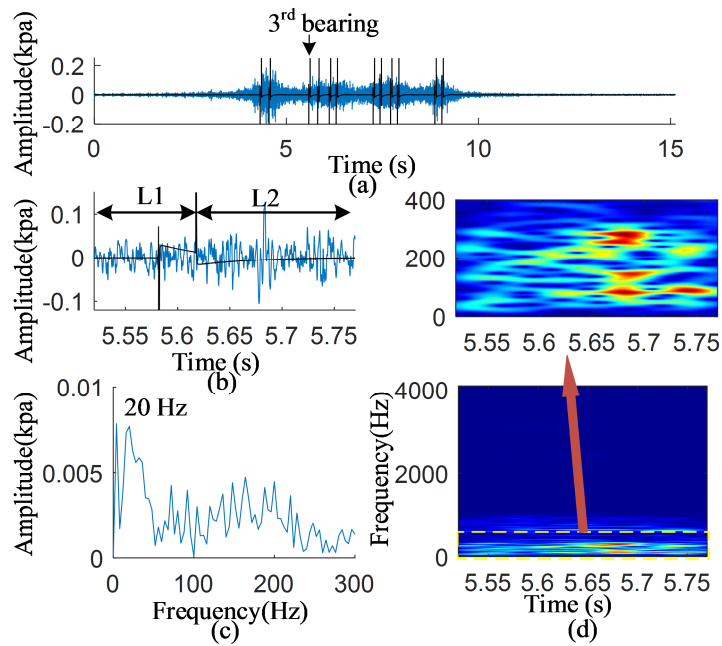

Fig. 13 Case 1 with the outer race fault: (a) the time domain waveform of the collected signal, (b) the time domain waveform of the 3rd bearing's analysis signal, (c) the Hilbert envelope spectrum of (b), (d) TFR of (b)

The ESCT method is applied to the analysis signal section of the field test recording. Fig. 14 shows 4 IF curves of the main harmonic components. The estimations of train speed, $\hat{v}$, their variances, σ, and the error rate of $\hat{v}_a$, ε, are obtained based on those IF curves using the ESCT method. An enhanced version of the multi-scale chirplet path pursuit (MSCPP) method is also applied in order to provide a comparison of performance, as presented in Tab. 6. The MSCPP method is an alternative to the SCT approach, which for this application must also be

enhanced using built-in criterions and variable digital filters [35]. The table shows that the values of σ and ε for the ESCT method are smaller than that for the enhanced MSCPP method. It demonstrates that the ESCT method can be used to obtain more stable results with comparably minor errors.

Tab. 6 Estimated values of motion parameters for the bearing with outer race fault

	$\hat{v}\,(h_1)$ m/s	$\hat{v}\,(h_2)$ m/s	$\hat{v}\,(h_3)$ m/s	$\hat{v}\,(h_4)$ m/s	σ	$\hat{v}_a$ m/s	ε %	$\hat{s}$ m
ESCT	11.57	14.04	13.64	13.59	1.24	13.21	0.84	1.33
(E)MSCPP	15.98	14.47	/	9.56	11.27	13.34	1.8	1.34

A series of VDFs are constructed and applied to the original signal to filter harmonic components using the ESCT method. The centre frequencies of those VDFs are the significant portions of IF curves. Thus, a residual of the original signal is obtained and passed to the TIR method in order to finally obtain the Doppler-free signal. The filtered signal is then obtained using the SK method with the ultimate result presented in Fig. 15. The time domain waveform, TFR and Hilbert envelope spectrum of the filtered signal are shown in Fig. 15 (a), (b) and (c), respectively. Fig. 15 (c) shows obvious peaks at f_{RPFO}, $2\,f_{RPFO}$ and $3\,f_{RPFO}$, which indicates the existence of an outer race fault.
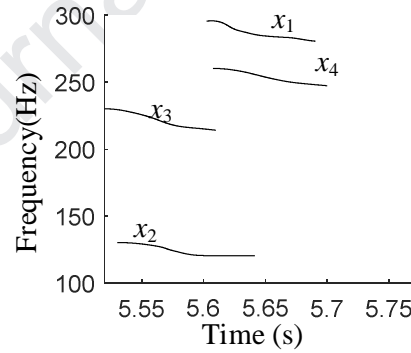

Fig. 14 IFs of harmonic components for field test for the bearing with outer race fault
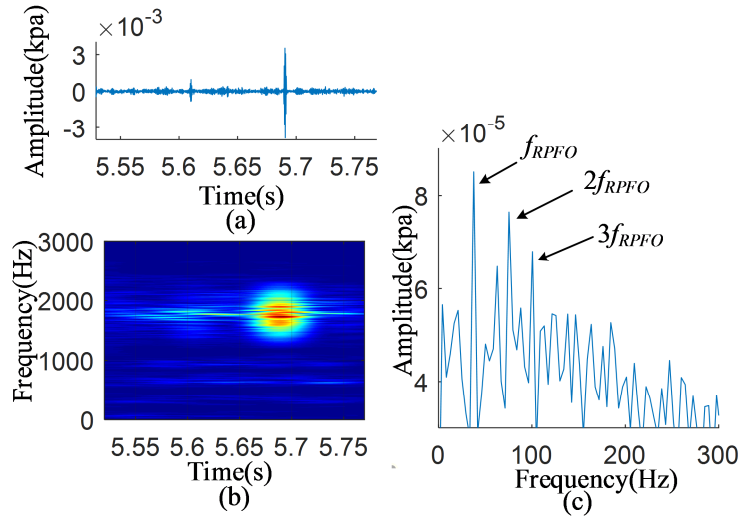
Fig. 15 SK result for the 3rd bearing in case 1: (a) time domain waveform of the filtered signal, (b) TFR of the filtered signal (c) Hilbert envelope spectrum of the filtered signal

To further verify the effectiveness of the proposed method, case 2 was conducted and the speaker broadcasted sound with roller fault information in the 3rd bearing. The collected acoustic signal in case 2 is shown as Fig. 16 (a). Fig. 16 (b) shows that the analysis signal that was recorded as the 3rd bearing passed the microphone, t_c=5.39 s. The Hilbert envelope spectrum and TFR of the analysis signal are shown in Fig. 16 (c) and (d). It can be seen from Fig. 16 (c) and (d) that there is significant harmonic interference and high-level noise present in the analysis signal to the extent that the fault feature is totally masked. The analysis signal is subjected to the proposed scheme and the result is shown in Fig. 17. Fig. 17 (a), (b) and (c) are the time domain waveform, TFR and Hilbert envelope spectrum of the filtered signal respectively. There are obvious peaks at f_{RFF} and $2f_{RFF}$ in Fig. 17 (c), which indicates the presence of a roller fault in the test bearing. The estimated motion parameters identified using the ESCT and enhanced MSCPP methods are demonstrated in Tab. 7. The table shows that the estimated values obtained using the ESCT method has smaller values of σ and ε than that those obtained using the enhanced MSCPP method, which is beneficial.

Tab. 7 Estimated values of motion parameters for the roller fault bearing

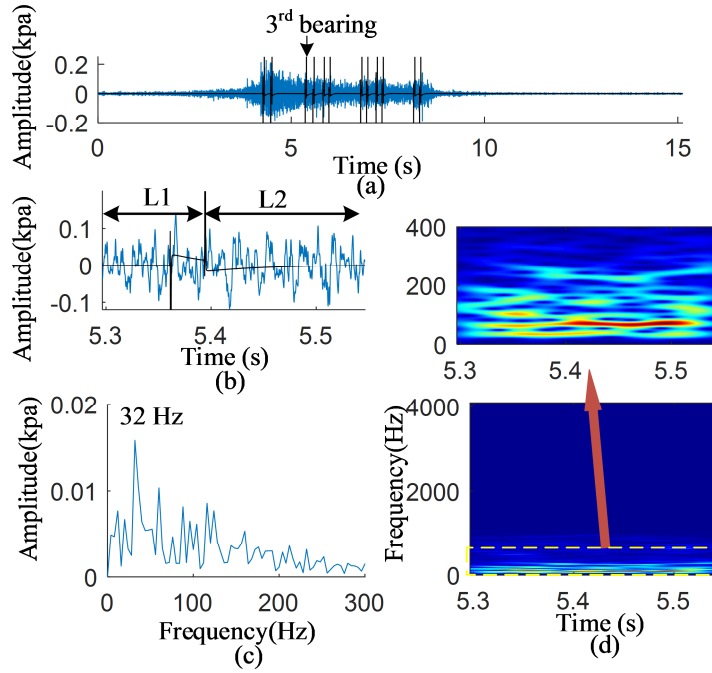|	$\hat{v}(h_1)$ m/s	$\hat{v}(h_2)$ m/s	$\hat{v}(h_3)$ m/s	σ	$\hat{v}_a$ m/s	ε %	$\hat{s}$ m
ESCT	12.73	13.23	13.47	0.14	13.14	0.3	1.32
(E)MSCPP	10.78	12.88	10.70	1.52	11.45	12.6	1.15

Fig. 16 Case 2 with the roller fault: (a) the time domain waveform of the collected signal, (b) the time domain waveform of the 3rd bearing's analysis signal, (c) the Hilbert envelope spectrum of (b), (d) TFR of (b)
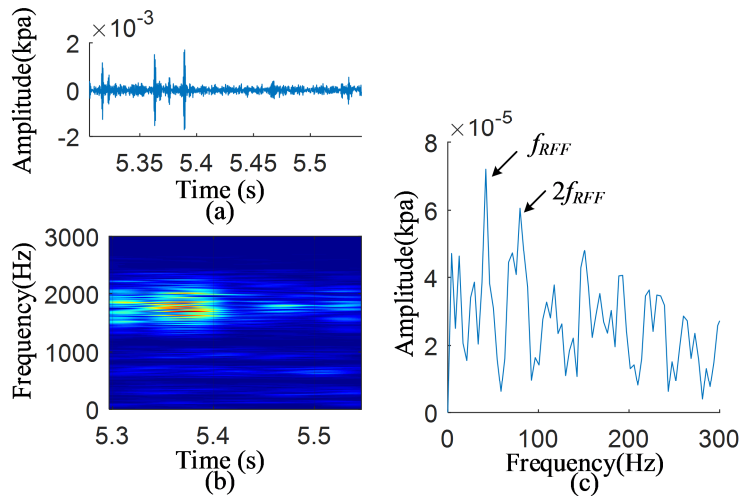

Fig. 17 SK result for the 3rd bearing in case 2: (a) time domain waveform of the filtered signal, (b) TFR of the filtered signal, (c) Hilbert envelope spectrum of the filtered signal

The proposed method was implemented for the 4th bearing in both cases. The SK results are shown in Fig. 18 and Fig. 19 for case 1 and case 2, respectively. Fig. 18 (c) is the Hilbert envelope spectrum of the filtered signal for the 4th bearing in case 1. There are no obvious peaks at f_{RPFO} and its harmonics. The similar situation occurred in Fig. 19 (c) which does not have obvious peaks at f_{RFF} and its harmonics. Hence, there is no fault information of outer

race fault and roller fault in the analysis signals of the 4th bearing in case 1 and case 2, respectively. Comparing with SK results for the 3rd bearing shown in Fig. 15 and Fig. 17, Fig. 18 and Fig. 19 further prove that the proposed method can be used to detect bearing faults effectively.
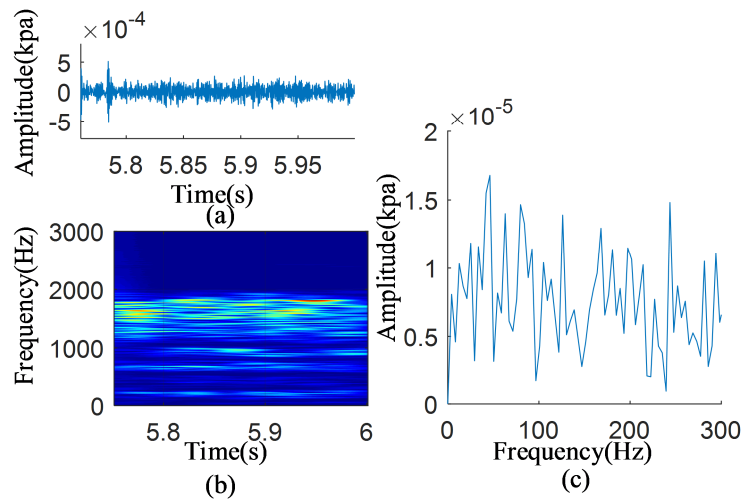

Fig. 18. SK result for the 4rd bearing in case 1: (a) time domain waveform of the filtered signal, (b) TFR of the filtered signal, (c) Hilbert envelope spectrum of the filtered signal
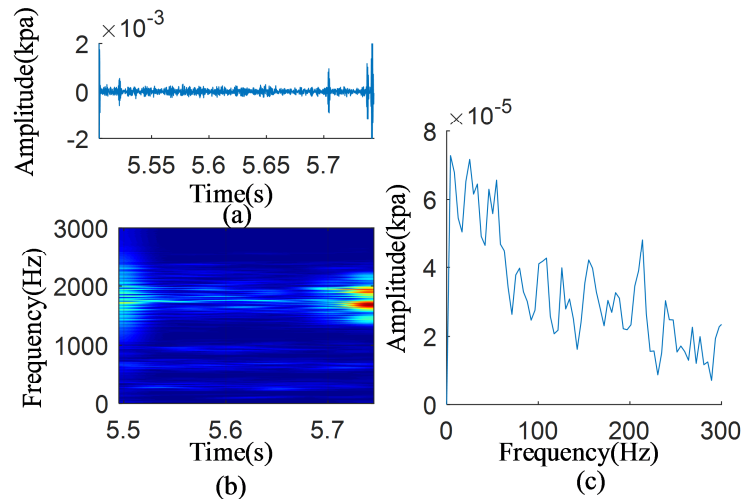

Fig. 19. SK result for the 4rd bearing in case 2: (a) time domain waveform of the filtered signal, (b) TFR of the filtered signal, (c) Hilbert envelope spectrum of the filtered signal

Conclusion

In this paper, a novel scheme based on an enhanced spline-kernelled chirplet transform (ESCT) method is proposed and used in wayside acoustic detection systems for train bearings. In the scheme, the ESCT method is proposed to identify and extract the significant portions

of IF curves. The obtained IF curves are then used to construct VDFs and estimate motion parameters of the test train simultaneously. The VDFs can be used to obtain residual signals through excluding harmonic components from the raw acoustic signal. The resampling time vector can be obtained to reduce Doppler Effect in the residual signal by using estimated motion parameters. The Doppler-free signal is finally subject to the SK method and hence the fault feature can be extracted. The simulation and field experiments were conducted to test the proposed method. From experiments' results, the below conclusions can be obtained.

- The results of the experiments demonstrate the effectiveness of the proposed scheme in wayside acoustic detection for train bearings. The ESCT method, at the core of the proposed scheme, has been shown to be more effective than equivalent enhanced MSCPP based approaches used previously.

- It has been shown that two criterions can be constructed to effectively identify the births and deaths of the significant portions of IFs using the ESCT method based on the energy contribution and Doppler Effect characteristics of IFs.

- The performance of the Doppler Effect reduction method is highly dependent on the accuracy of IF curve extraction. The noise level in the collected signal has a significant influence on estimating IFs. Thus, de-noising methods should be the subject of further research.

- One pair of light-gates is still used to identify the target bearing and the detection zone. Ultimately, systems with only the acoustic sensors would be preferable. Hence an acoustic trigger for the system may also be the subject of future research.

Acknowledgements

Reference

[1]   Y. Li, X. Liang, J. Lin, Y. Chen, and J. Liu, Train axle bearing fault detection using a feature selection scheme based multi-scale morphological filter, Mechanical Systems and Signal Processing.101 (2018) 435-448.

[2] D. Zhang, E. Mani, S. Edward, R. Clive, and D. Yu, Adaptive fault feature extraction from wayside acoustic signals from train bearings, Journal of Sound and Vibration.425 (2018) 221-238.

[3] J. Ding, W. Zhao, B. Miao, and J. Lin, Adaptive sparse representation based on circular-structure dictionary learning and its application in wheelset-bearing fault detection, Mechanical Systems and Signal Processing 111(1) (2018) 399-422.

[4] J. Dybała and S. Radkowski, Reduction of Doppler effect for the needs of wayside condition monitoring system of railway vehicles, Mechanical Systems and Signal Processing.38(1) (2013) 125-136.

[5] C. Yiakopoulos, J. Maczak, K. Rodopoulos and I. Antoniadis, Multicomponent decomposition of a time-varying acoustic Doppler signal generated by a passing railway vehicle using Complex Shifted Morlet Wavelets, Transportation Research Part C: Emerging Technologies.44 (2014) 34-51.

[6] Q. He , J. Wang, F. Hu , and F. Kong, Wayside acoustic diagnosis of defective train bearings based on signal resampling and information enhancement, Journal of Sound and Vibration.332(21) (2013) 5635–5649.

[7] S. Zhang, Q. He, K. Ouyang, and W. Xiong, Multi-bearing weak defect detection for wayside acoustic diagnosis based on a time-varying spatial filtering rearrangement., Mechanical Systems and Signal Processing.100 (2018) 224-241.

[8] Q. He, J. Wang, F. Hu, and F. Kong, Wayside acoustic diagnosis of defective train bearings based on signal resampling and information enhancement, Journal of Sound and Vibration.332(21) (2013) 5635-5649.

[9] F. Liu, C. Shen, Q. He, A. Zhang, F. Kong, and Y. Liu, Doppler effect reduction scheme via acceleration-based Dopplerlet transform and resampling method for the wayside acoustic defective bearing detector system, Proceedings of the Institution of Mechanical Engineers, Part C: Journal of Mechanical Engineering Science.228(18) (2014) 3356-3373.

[10] C. Wang, C. Shen, Q. He, A. Zhang, F. Liu, and F. Kong, Wayside acoustic defective bearing detection based on improved Dopplerlet transform and Doppler transient matching, Applied Acoustics 101(2016) 141-155.

[11] C. Wang, C. Shen, Q. He, A. Zhang, F. Liu, and F. Kong, Wayside acoustic defective bearing detection based on improved Dopplerlet transform and Doppler transient matching, Applied Acoustics.101(2016) 141-155.

[12] S. Zhang, Q. He, H. Zhang, and K. Ouyang, Doppler Correction Using Short-Time MUSIC and Angle Interpolation Resampling for Wayside Acoustic Defective Bearing Diagnosis, IEEE Transactions on Instrumentation and Measurement.4 (2017) 671-680.

[13] C. Wang, F. Hu, Q. He, A. Zhang, F. Liu, and F. Kong, De-noising of wayside acoustic signal from train bearings based on variable digital filtering, Applied Acoustics 83 (2014) 127-140.

[14] C. Wang, F. Kong, Q. He, F. Hu, and F. Liu, Doppler Effect removal based on instantaneous frequency estimation and time domain re-sampling for wayside acoustic defective bearing detector system, Measurement.50 (2014) 346-355.

[15] H. Zhang, S. Lu, Q. He, and F. Kong, Multi-bearing defect detection with trackside acoustic signal based on a pseudo time–frequency analysis and Dopplerlet filter, Mechanical Systems and Signal Processing 70 (2016) 176-200.

[16] H. Zhang , S. Zhang , Q. He , and F. Kong The Doppler Effect based acoustic source separation for a wayside train bearing monitoring system, Journal of Sound and Vibration.361(20) (2016) 307–329.

[17] N. G. De Bruijn, Uncertainty principles in Fourier analysis, Inequalities 2(1) (1967) 57-71.

[18] Y. Yang, Z. Peng, W. Zhang, and G. Meng, Frequency-varying group delay estimation using frequency domain polynomial chirplet transform, Mechanical Systems and Signal Processing.46(1) (2014) 146-162.

[19] F. Auger and P. Flandrin, Improving the readability of time-frequency and time-scale representations by the reassignment method, IEEE Transactions on signal processing 43(5) (1995) 1068-1089.

[20] I. Daubechies, J. Lu, and H. Wu, Synchrosqueezed wavelet transforms: An empirical mode decomposition-like tool, Applied and computational harmonic analysis 30(2) (2011) 243-261.

[21] G. Yu, M. Yu, and C. Xu, Synchroextracting Transform, IEEE Transactions on Industrial Electronics.64(10) (2017) 8042-8054.

[22] Z. Peng, G. Meng, F. Chu, Z. Lang, W. Zhang, and Y. Yang, Polynomial chirplet transform with application to instantaneous frequency estimation, IEEE Transactions on Instrumentation and Measurement 60(9) (2011) 3222-3229.

[23] Y. Yang, Z. Peng, G. Meng, and W. Zhang, Characterize highly oscillating frequency modulation using generalized Warblet transform, Mechanical Systems and Signal Processing 26(1) (2012) 128-140.

[24] Y. Yang, Z. Peng, G. Meng, and W. Zhang, Spline-kernelled chirplet transform for the analysis of signals with time-varying frequency and its application, IEEE Transactions on Industrial Electronics.59(3) (2012) 1612-1621.

[25] H. Timlelt, Y. Remram, and A. Belouchrani, Closed-form solution to motion parameter estimation of an acoustic source exploiting Doppler effect, Digital Signal Processing.63 (2017) 35-43.

[26] F. Peng, D. Yu, and J. Luo, Sparse signal decomposition method based on multi-scale chirplet and its application to the fault diagnosis of gearboxes, Mechanical Systems and Signal Processing.25(2) (2011) 549-557.

[27] J. Luo, D. Yu, and M. Liang, Application of multi-scale chirplet path pursuit and fractional Fourier transform for gear fault detection in speed up and speed-down processes, Journal of sound and vibration.331(22) (2012) 4971-4986.

[28] F. Liu, Q. He, F. Kong, and Y. Liu, Doppler effect reduction based on time-domain interpolation resampling for wayside acoustic defective bearing detector system, Mechanical Systems and Signal Processing.46(2) (2014) 253-271.

[29] J. H. Ahlberg, E.N. Nilson and J.L. Walsh, The Theory of Splines and Their Applications: Mathematics in Science and Engineering: A Series of Monographs and Textbooks, Elsevier, New York, 2016.

[30] P. Morse and K. Ingard, Theoretical acoustics, McGraw Hill, Princeton, USA, 1986.

[31] W. Yang, P. J. Tavner, and W. Tian, Wind turbine condition monitoring based on an improved spline-kernelled Chirplet transform, IEEE Transactions on Industrial Electronics.62(10) (2015) 6565-6574.

[32] Y. Yang, W. Zhang, Z. Peng, and Z. Meng, Multicomponent signal analysis based on polynomial chirplet transform, IEEE Transactions on Industrial Electronics.60(9) (2013) 3948-3956.

[33] C. Wu, J. Liu, F. Peng, D. Yu, and R. Li, Gearbox fault diagnosis using adaptive zero phase time-varying filter based on multi-scale chirplet sparse signal decomposition, Chinese Journal of Mechanical Engineering.26(4) (2013) 831-838.

[34] M. Entezami, E. Stewart, J. Tutcher, W. Driscoll, R. Ellis, G. Yeo, Z. Zhang, C. Roberts, T. Kono, and S. Bayram, Acoustic analysis techniques for condition monitoring of roller bearings. in Railway Condition Monitoring, RCM 2014, Birmingham, 2014, 1-8.

[35]   D. Zhang, M. Entezami, E. Stewart, C. Roberts, and D. Yu, A novel Doppler Effect reduction method for wayside acoustic train bearing fault detection systems, Applied Acoustics.145 (2019) 112-124.

- A novel scheme is proposed for wayside acoustic detection of train bearings;

- An ESCT method is proposed to extract multiple components and their IFs;

- Two build-in criterions in ESCT are proposed to identify births and deaths of IFs;

- Motion parameters are estimated by using information of interference components;

- Simulation and field experiments verify the effectiveness of the proposed method.

Declaration of interests

■ The authors declare that they have no known competing financial interests or personal relationships that could have appeared to influence the work reported in this paper.

☐The authors declare the following financial interests/personal relationships which may be considered as potential competing interests: